Friction, nanostructure, and residual stress of single-layer and multi-layer amorphous carbon films deposited by radio-frequency sputtering

J. Xie and K. Komvopoulos
Department of Mechanical Engineering, University of California, Berkeley, California 94720

Abstract

Single- and multi-layer amorphous carbon (*a*-C) films of varying thickness and surface roughness were deposited on Si(100) substrates by radio-frequency sputtering in a pure Ar atmosphere. The thickness, roughness, coefficient of friction, and residual stress of the *a*-C films were measured by profilometry, atomic force microscopy, surface force microscopy, and curvature method, respectively. The through-thickness nanostructure and elemental composition of the films were examined by cross-sectional transmission electron microscopy and electron energy loss spectroscopy. The multi-layer *a*-C films were found to exhibit lower roughness, coefficient of friction, and residual stress and higher tetrahedral carbon atom hybridization than single-layer *a*-C films of similar thickness. The results of this study reveal a strong correlation of the friction characteristics with the surface roughness and nanostructure of both single- and multi-layer *a*-C films.

1. INTRODUCTION

Amorphous carbon (*a*-C) films are extensively used as protective overcoats in numerous applications, mainly due to their excellent physical properties and chemical inertness. Among various film deposition techniques,[1–4] radio-frequency (rf) sputtering is a widely used film deposition method because the film precursors (i.e., carbon atoms and/or clusters of atoms) require low input energy compared to deposition methods using energetic ions as film-forming precursors. Moreover, inert ion bombardment of the film surface during sputtering enables the film properties to be tailored without changing the film chemical environment. Energetic Ar^+ ion bombardment of the growing film is commonly used in sputtering to enhance the film density and hardness;[4–6] however, ion bombardment usually produces films possessing high residual stress and different microstructures, depending on the competing kinetic processes encountered under nonequilibrium film-growth conditions.[4,7–9] Previous studies have shown that ion bombardment may produce compressive residual stresses up to about –16 GPa,[7,9,10] which may result in film delamination, buckling, agglomeration (clustering), and other adhesion failures when the film is grown to a critical thickness.[8,10,11] Therefore, preventing the development of high residual (intrinsic) stresses in films deposited under sputtering conditions of energetic ion bombardment is critical to the maximum film thickness.

Because the film roughness and friction characteristics affect the tribological performance of contacting surfaces, methods of depositing relatively smooth and hard films are of particular importance. Several methods have been used to prevent the development of undesirable high residual stresses in carbon films, such as post-process treatment like thermal annealing,[12–15] addition of various elements (e.g., Si, Al, W, and Ti) to modify the film structure,[16–21] and deposition of multi-layer films consisting of alternating hard/soft *a*-C layers.[24,25]

The structure and properties of sputtered *a*-C films greatly depend on deposition conditions. For example, ultrathin *a*-C films with sp^3 contents of ~50 at% and nanohardness as high as ~39 GPa can be synthesized under optimum conditions of absorbed rf power, substrate bias voltage, working pressure, and

gas flow rate.[4] The substrate bias voltage is of particular importance because it controls the kinetic energy of bombarding Ar^+ ions. The very low roughness and high hardness of *a*-C films synthesized under rf sputtering conditions of optimum substrate bias voltage (typically, –200 V) may be attributed to the competing effects of ion bombardment, re-sputtering, and irradiation damage by the highly energetic Ar^+ ions.[4,22,23]

The deposition of multi-layer *a*-C films comprising alternating hard/soft ultrathin carbon layers has been the objective of several previous studies. The low residual stress of multi-layer carbon films consisting of alternating sp^2- and sp^3-rich carbon layers has been attributed to stress relaxation induced by the soft (sp^2) buffer layers;[24] however, X-ray photoelectron spectroscopy (XPS) used in the former study to examine the cross-sectional structure of the ultrathin layers comprising the film has limited resolution for nanoscale structural analysis. Nanoindentation, XPS, and X-ray reflectivity (XRR) studies[25,26] of the microstructure and nanomechanical properties of multi-layer films consisting of alternating soft/hard *a*-C layers (deposited under rf sputtering conditions of zero (or floating) and –200 V substrate bias voltage, respectively) showed a film hardness of ~20 GPa, mass density of soft and hard layers equal to 2.0–2.2 and 2.5 g/cm^3, respectively, and an average sp^3 content of ~46 at%. Although the growth and physical properties of single *a*-C films deposited by rf sputtering have been thoroughly studied, a comprehensive analysis of the cross-sectional nanostructure of multi-layer soft/hard *a*-C films has not been reported.

The main objective of this study is to investigate the friction characteristics and nanostructure of multi-layer *a*-C films and compare them to those of single-layer *a*-C films deposited under similar rf sputtering conditions. The interdependence of surface morphology (roughness), friction properties (coefficient of friction), cross-sectional nanostructure (sp^2 and sp^3 hybridization), and residual stress is examined in the context of atomic force microscopy (AFM), surface force microscopy (SFM), transmission electron microscopy (TEM), and electron energy loss spectroscopy (EELS) results.

II. EXPERIMENTAL METHODS

A. Film deposition

Single- and multi-layer *a*-C films of different thickness were deposited on smooth Si(100) substrates (root-mean-square (rms) roughness ≈ 0.1 nm) by sputtering a high-purity (~99.99%) graphite target with Ar^+ ions in a low-pressure sputtering system (Randex-2400 model, Perkin-Elmer). Before film deposition, the graphite target was cleaned by sputter-etching for 15 min and then the Si(100) substrate was sputtered for 3 min under conditions of forward rf power P_f = 250 W, working pressure p = 3 mTorr, and Ar gas flow rate f = 20 sccm to produce a clean and oxygen-free silicon surface. The multi-layer film comprised five alternating hard/soft ultrathin *a*-C layers, with the first layer deposited onto the Si(100) substrate and the last (top) layer being hard *a*-C layers. All depositions were performed in a pure Ar atmosphere under sputtering conditions of P_f = 750 W and p = 3 mTorr. Soft and hard *a*-C layers were synthesized under a substrate bias voltage V_s = 0 and –200 V, respectively. Besides the substrate bias voltage, all other deposition parameters of soft and hard *a*-C layers were identical. Single-layer *a*-C film deposition was performed under the same plasma discharge conditions with the hard layers of the multi-layer films (i.e., V_s = –200 V). The aforementioned plasma discharge conditions have been found to produce *a*-C films exhibiting optimum properties.[4,10] For single-layer *a*-C films, the deposition time was t ≈ 4, 6, and 12 min, corresponding to a film thickness h ≈ 30, 60, and 120 nm, respectively. To obtain a total deposition time equal to that of single-layer *a*-C films of thickness h ≈ 30, 60, and 120 nm, the deposition time of the soft and hard layers of the multi-layer *a*-C films was set at 36, 72, and 144 s, respectively.

B. Atomic force microscopy

The film surface roughness was determined from 2 × 2 μm^2 images acquired with an AFM (NanoScope II, Digital Instruments) operated in tapping mode. The film roughness was calculated as the mean value of at least four measurements obtained from different AFM surface images of each film. All

the AFM images were obtained with Si tips having a nominal radius of curvature equal to ~10 nm.

C. Tribomechanical testing

The coefficient of friction of the synthesized *a*-C films was measured with a surface force microscope (SFM) consisting of a force transducer (Triboscope, Hysitron) interfaced with an AFM (NanoScope Ⅱ, Digital Instruments). The friction experiments were performed with a conical diamond tip having a nominal radius of curvature equal to ~20 μm, using a normal force in the range of 50–1200 μN, a constant sliding speed of 0.4 μm/s, and a lateral displacement (sliding distance) equal to 4 μm. The coefficient of friction was calculated as the ratio of the measured lateral (friction) force to the applied normal force. For statistical analysis, at least five indentations were performed at different locations of each film surface and 300 coefficient of friction measurements obtained along the sliding track were used to calculate the steady-state coefficient of friction.

D. Residual stress measurement

The residual stress in the films was determined from the sample curvature measured with a Flexus (Tencor FLX-2320) system. For these measurements, 4-inch-diameter p-type Si(100) wafers were coated with 60-nm-thick *a*-C films synthesized under deposition conditions identical to those of single- and multi-layer *a*-C films of same thickness. The residual stress σ in the films was calculated from Stoney's equation

$$\sigma = \left(\frac{E}{1-\nu}\right)\frac{d^2}{6Rh} \quad (1)$$

where $E/(1-\nu)$ is the biaxial elastic modulus of the substrate (equal to 180.5 GPa for Si(100)), d and h are the substrate and film thickness, respectively, and R is the measured radius of curvature of the carbon-coated Si(100) substrate.

E. Microanalysis methods

Cross-sectional samples for high-resolution transmission electron microscopy (HRTEM) were prepared by mechanical grinding, dimpling, and surface finishing by ion milling. A 5- to 10-nm-thick Au

capping layer was sputtered onto each sample surface before bonding to enhance the distinction of the *a*-C film from the epoxy glue and to separate the EELS carbon signal from carbon-based epoxy glue. More details about the TEM sample preparation method used in this study can be found elsewhere.[27,28]

HRTEM images and EELS spectra were obtained with an FEI Tecnai (F20 UT) microscope operated at 200 kV, using a CCD camera (2048 × 2048 pixels) positioned 42 mm behind the Gatan imaging filter. The EELS collection semi-angle was set at 16.3 mrad. A 9.4 mrad C2 semi-angle and a 150 μm C2 aperture were used in the present study. The spatial resolution of the scanning TEM (STEM) without a monochromator is equal to 0.14 nm. Using the full-width at half-maximum of the zero-loss peak, the energy resolution was found to be ≤0.58 eV. Considering that the band gap difference between sp^2 and sp^3 is about 0.8–0.9 eV, this energy resolution is sufficiently low for distinguishing sp^2 from sp^3 hybridizations.

III. RESULTS AND DISCUSSION

Figure 1 shows that, for a fixed forward rf power, the thickness of both single- and multi-layer *a*-C films varies linearly with the deposition time, in accord with previous studies.[22,23] The close agreement of the data implies a similar deposition rate of ~9.2 nm/min for both types of *a*-C films deposited under the present sputtering conditions.

Figure 2 shows the variation of the coefficient of friction of single- and multi-layer *a*-C films with the normal force and film thickness. The results indicate that in the low-force range (i.e., <600 μN) the coefficient of friction decreases with the increase of the normal force in a nonlinear fashion. This trend indicates predominantly elastic deformation under sliding conditions of normal force <600 μN. It is well-known that the friction coefficient of elastic spherical contacts is inversely proportional to the cubic root of the normal force and that the friction force is mainly due to adhesion and roughness effects.[29] Figure 3 shows a log-log plot of the coefficient of friction of ~120-nm-thick single-layer *a*-C films versus normal force. The slope of the best-fit line shown in Fig. 3 is equal to –0.34, confirming the dominance of elastic

deformation at the sliding interface in the low-force range (<600 μN).

Figure 2 also shows that the multi-layer *a*-C films consistently demonstrate lower friction than the single-layer *a*-C films regardless of the film thickness. This result may be explained by considering the surface roughness effect on friction. Figures 4(a) and 4(b) show the coefficient of friction and rms roughness of single- and multi-layer *a*-C films versus film thickness, respectively, for a normal force of 150 μN. The coefficient of friction of both film types increases with the rms roughness; however, the rougher single-layer films yield significantly higher coefficients of friction than the multi-layer films.

Figure 5 shows cross-sectional HRTEM images of single- and multi-layer *a*-C films of total thickness equal to ~60 nm. Figures 5(a) and 5(c) show overall cross-sectional views, while Figs. 5(b) and 5(d) show high-magnification images of the interface between the Si(100) substrate and the bottom of *a*-C films. The single-layer film shows an overall uniform thickness (Fig. 5(a)), whereas the multi-layer film consists of five alternating hard/soft *a*-C layers distinguished by contrast differences (the three hard layers are darker than the two soft layers) (Fig. 5(c)). High-magnification images reveal the formation of crystalline nanodomains in both single- and multi-layer *a*-C films (e.g., circled areas in Figs. 5(b) and 5(d), respectively). The formation of crystalline nanodomains has also been observed in a previous TEM study and have been attributed to carbon atom clusters ejected from the graphite target by the bombarding Ar^+ ions.[27] In addition, an intermixing ultrathin layer (~2–3 nm thick) can be observed at the interface of both films with the crystalline Si(100) substrate, also in agreement with previous findings.[27]

The cross-sectional elemental composition of the *a*-C films can be interpreted in the context of analytical EELS results. The energy of electrons traveling through a specimen lost due to inelastic electron-electron collisions obtained from EELS[30,31] can be used to determine the chemical composition and nanostructure. Beam electrons interacting with electrons of the conduction and/or valence bands of the specimen material are detected in the low-energy loss range (<50 eV) of the EELS spectrum, whereas information about inelastic interactions between beam electrons and inner (core-shell) electrons can be deduced from the high-energy loss range (>50 eV). Thus, information about the elemental composition

can be obtained from ionization edges.

Carbon K-edge EELS spectra in the range of 280–305 eV were analyzed to determine the sp^2 and sp^3 contents of the *a*-C films, using the pre-edge peak at 285 eV, which is due to electron excitation from the ground-state 1s core levels to the vacant π^*-like anti-bonding states, and the edge from 290 eV, which is due to electron excitation to the higher σ^* states.[32] The π^* peak is fitted with a Gaussian distribution, whereas the σ^* peak is integrated over the small energy range of 290–305 eV to minimize plural scattering effects. Since the area ratio of these two peaks is proportional to the relative number of π^* and σ^* orbitals, which is 0/4 for 100% sp^3 and 1/3 for 100% sp^2, the fraction of sp^2 bonded carbon atoms x in the film can be obtained by[32]

$$\frac{(\pi^*/\sigma^*)_{\text{film}}}{(\pi^*/\sigma^*)_{\text{std}}} = \frac{3x}{4-x} \qquad (2)$$

where the standard (std) sample is an evaporated carbon film consisting of 100% sp^2. More details about the curve fitting method and the calculation of the sp^3 fraction are given elsewhere.[33]

Figures 6(a) and 6(b) show the through-thickness structure of ~60-nm-thick single- and multi-layer *a*-C films, respectively. The normalized carbon intensity was obtained by integrating the EELS spectrum from 280 to 305 eV, while the sp^3 depth profiles were calculated from the C K-edge spectra using Eq. (2). The carbon atom concentration and sp^3 distribution through the film thickness reveal the existence of different regions. Figure 6(a) indicates that the single-layer *a*-C film comprises the following four distinct regions: (i) *crystalline substrate* (the carbon signal intensity is almost zero because the substrate consists of silicon); (ii) *interface layer* (both the carbon concentration and the sp^3 content increase sharply); (iii) *bulk film* (almost constant carbon concentration and sp^3 content); (iv) *surface layer* (both the carbon concentration and the sp^3 fraction decrease sharply). Figure 6(b) shows that within the bulk layer of the multi-layer *a*-C film, the carbon intensity changes periodically. The carbon intensity shows a positive slope in the hard layers and a negative slope in the soft layers, whereas the sp^3 fraction remains almost constant and there are no obvious differences between hard and soft layers.

Table I shows a comparison between results of the total film thickness (measured from TEM and EELS), rms roughness, coefficient of friction, average sp^3 content of the bulk layer, and residual stress (Eq. (1)) of ~60-nm-thick single- and multi-layer *a*-C films. The sum of the thicknesses of all the layers (i.e., intermixing, bulk, and surface layers) is referred to as the total thickness. The agreement between TEM and EELS results is fairly good. Also the results of the sp^3 content are in agreement with previous findings.[27] The surface roughness of multi-layer films is ~50% lower than that of the single-layer films, consistent with the lower coefficient of friction of multi-layer *a*-C films in the low range of normal force (Fig. 2). The similar sp^3 contents of single- and multi-layer films are also consistent with the similar coefficients of friction in the high normal force range (Fig. 2), where plastic shearing (plowing) is the dominant mode of deformation. Film plastic shearing greatly depends on the film nanostructure, particularly the type of carbon atom bonding. Since the sp^3 fraction controls the nanomechanical properties, the single- and multi-layer films should exhibit similar plastic shear resistance, which explains the similar coefficients of friction in the high normal force range (i.e., >600 μN). In addition, despite the slightly higher sp^3 content of the bulk layer of multi-layer *a*-C films, the residual stress in these films is ~55% lower than that in single-layer *a*-C films. Thus, rf sputtering of alternating hard (V_s = –200 V) and soft (V_s = 0) ultrathin (~10 nm) *a*-C layers produces smoother carbon films possessing lower friction and significantly reduced residual stress and preserves the overall nanostructure (hybridization state) compared to single-layer films of same thickness deposited under the same sputtering conditions.

IV. CONCLUSIONS

The deposition rate, roughness, coefficient of friction, and nanostructure of single- and multi-layer *a*-C films were examined in the light of profilometry, AFM, SFM, HRTEM, and EELS results. The multi-layer films synthesized under low-pressure plasma discharge conditions of substrate bias voltage of 0 V (soft layers) and –200 V (hard layers) demonstrate smoother surface topographies, lower coefficient of friction, significantly reduced residual stress, and slightly higher sp^3 content compared to single-layer

a-C films deposited under –200 V substrate bias voltage. Sliding under a normal force of <600 μN resulted in predominantly elastic deformation of both films; however, the multi-layer films exhibited significantly lower friction than single-layer films of similar thickness. TEM revealed the existence of crystalline nanodomains in both films, whereas EELS confirmed the existence of a layered structure consisting of intermixing, bulk, and surface layers. The results of this study show that the surface roughness, friction, and residual stress of rf sputtered *a*-C films can be greatly reduced by depositing alternating hard and soft ultrathin *a*-C layers.

ACKNOWLEDGMENTS

This research was funded by the Computer Mechanics Laboratory (CML), University of California, Berkeley. The TEM/EELS studies were carried out at the National Center for Electron Microscopy, Molecular Foundry, Lawrence Berkeley National Laboratory (Proposal No. 1886). Work at the Molecular Foundry is supported by the Office of Science, Office of Basic Energy Sciences, U.S. Department of Energy (Contract No. DE-AC02-05CH11231).

REFERENCES

[1] J. Ishikawa, Y. Takeiri, K. Ogawa, and T. Takagi: Transparent carbon film prepared by mass-separated negative–carbon-ion-beam deposition. *J. Appl. Phys.* **61**, 2509 (1987).

[2] D.R. McKenzie, D. Muller, and B.A. Pailthorpe: Compressive-stress-induced formation of thin-film tetrahedral amorphous carbon. *Phys. Rev. Lett.* **67**, 773 (1991).

[3] P. Kovarik, E.B.D. Bourdon, and R.H. Prince: Electron-energy-loss characterization of laser-deposited *a*-C, *a*-C:H, and diamond films. *Phys. Rev. B* **48**, 12123 (1993).

[4] W. Lu and K. Komvopoulos: Dependence of growth and nanomechanical properties of ultrathin amorphous carbon films on radio frequency sputtering conditions. *J. Appl. Phys.* **86**, 2268 (1999).

[5] Y. Lifshitz, G.D. Lempert, and E. Grossman: Substantiation of subplantation model for diamondlike film growth by atomic force microscopy. *Phys. Rev. Lett.* **72**, 2753 (1994).

[6] J. Schwan, S. Ulrich, T. Theel, H. Roth, H. Ehrhardt, P. Becker, and S.R.P. Silva: Stress-induced formation of high-density amorphous carbon thin films. *J. Appl. Phys.* **82**, 6024 (1997).

[7] J. Schwan, S. Ulrich, H. Roth, E. Ehrhardt, S.R.P. Silva, J. Robertson, R. Samlenski, and R. Brenn: Tetrahedral amorphous carbon films prepared by magnetron sputtering and dc ion plating. *J. Appl. Phys.* **79**, 1416 (1996).

[8] M. Ohring: *The Materials Science of Thin Films*. Academic Press, Boston, MA, 1992.

[9] W. Lu and K. Komvopoulos: Implanted argon atoms as sensing probes of residual stress in ultrathin films. *Appl. Phys. Lett.* **76**, 3206 (2000).

[10] W. Lu, K. Komvopoulos, and S.W. Yeh: Stability of ultrathin amorphous carbon films deposited on smooth silicon substrates by radio frequency sputtering. *J. Appl. Phys.* **89**, 2422 (2001).

[11] D.J. Srolovitz and M.G. Goldiner: The thermodynamics and kinetics of film agglomeration. JOM (TMS) **47**, 31 (1995).

[12] T.A. Friedmann, J.P. Sullivan, J.A. Knapp, D.R. Tallant, D.M. Follstaedt, D.L. Medlin, and P.B. Mirkarimi: Thick stress-free amorphous-tetrahedral carbon films with hardness near that of diamond. *Appl. Phys. Lett.* **71**, 3820 (1997).

[13] A.C. Ferrari, B. Kleinsorge, N.A. Morrison, A. Hart, V. Stolojan, and J. Robertson: Stress reduction and bond stability during thermal annealing of tetrahedral amorphous carbon. *J. Appl. Phys.* **85**, 7191 (1999).

[14] R. Kalish, Y. Lifshitz, K. Nugent, and S. Prawer: Thermal stability and relaxation in diamond-like-carbon. A Raman study of films with different sp^3 fractions (*ta*-C to *a*-C). *Appl. Phys. Lett.* **74**, 2936 (1999).

[15] J.P. Sullivan, T.A. Friedmann, and A.G. Baca: Stress relaxation and thermal evolution of film properties in amorphous carbon. *J. Electron. Mater.* **26**, 1021 (1997).

[16] M. Chhowalla, Y. Yin, G.A.J. Amaratunga, D.R. McKenzie, and T. Fauenheim: Highly tetrahedral amorphous carbon films with low stress. *Appl. Phys. Lett.* **69**, 2344 (1996).

[17] W. Dai and A. Wang: Deposition and properties of Al-containing diamond-like carbon films by a hybrid ion beam sources. *J. Alloys Compd.* **509**, 4626 (2011).

[18] C.S. Lee, K.-R. Lee, K.Y. Eun, K.H. Yoon, J.H. Han: Structure and properties of Si incorporated tetrahedral amorphous carbon films prepared by hybrid filtered vacuum arc process. *Diam. Relat. Mater.* **11**, 198 (2002).

[19] A.-Y. Wang, K.-R. Lee, J.-P. Ahn, J.H. Han: Structure and mechanical properties of W incorporated diamond-like carbon films prepared by a hybrid ion beam deposition technique. *Carbon* **44**, 1826 (2006).

[20] B. Shi and W.J. Meng: Intrinsic stresses and mechanical properties of Ti-containing hydrocarbon coatings. J. Appl. Phys. **94**, 186 (2003).

[21] P. Zhang, B.K. Tay, C.Q. Sun, and S.P. Lau: Microstructure and mechanical properties of nanocomposite amorphous carbon films. J. Vac. Sci. Technol. A **20**, 1390 (2002).

[22] D. Wan and K. Komvopoulos: Effect of low-pressure plasma discharge conditions on the thickness and roughness of ultrathin films of amorphous carbon. *J. Appl. Phys.* **100,** 063307 (2006).

[23] J. Xie and K. Komvopoulos: Hybridization and tribomechanical properties of ultrathin amorphous carbon films synthesized by radio-frequency low-pressure plasma discharges. *Surf. Coat. Technol.* **262**, 15 (2015).

[24] S. Logothetidis, C. Charitidis, M. Gioti, Y. Panayiotatos, M. Handrea, and W. Kautek: Comprehensive study on the properties of multilayered amorphous carbon films. *Diam. Relat. Mater.* **9**, 756 (2000).

[25] W. Lu, K. Komvopoulos, P. Patsalas, C. Charitidis, M. Gioti, and S. Logothetidis: Microstructure and nanomechanical and optical properties of single-and multi-layer carbon films synthesized by radio frequency sputtering. *Surf. Coat. Technol.* **168**, 12 (2003).

[26] P. Patsalas, S. Logothetidis, and P.C. Kelires: Surface and interface morphology and structure of

amorphous carbon thin and multilayer films. *Diam. Relat. Mater.* **14**, 1241 (2005).

[27] D. Wan and K. Komvopoulos: Transmission electron microscopy and electron energy loss spectroscopy analysis of ultrathin amorphous carbon films. *J. Mater. Res*. **19**, 2131 (2004).

[28] N. Wang and K. Komvopoulos: Incidence angle effect of energetic carbon ions on deposition rate, topography, and structure of ultrathin amorphous carbon films deposited by filtered cathodic vacuum arc. *IEEE Trans. Magn*. **48**, 2220 (2012).

[29] W. Lu and K. Komvopoulos: Nanotribological and nanomechanical properties of ultrathin amorphous carbon films synthesized by radio frequency sputtering. *ASME J. Tribol.* **123**, 641 (2001).

[30] D.B. Williams and C.B. Carter, *Transmission Electron Microscopy: A Textbook for Materials Science* (Springer, New York, 2009), ch. 37, pp. 679–681.

[31] R.F. Egerton, *Electron Energy-Loss Spectroscopy in the Electron Microscope* (3rd ed., Springer, New York, 2011), ch. 3, pp. 111–229.

[32] J.J. Cuomo, J.P. Doyle, J. Bruley, and J.C. Liu: Sputter deposition of dense diamond-like carbon films at low temperature. *Appl. Phys. Lett*. **58**, 466 (1991).

[33] N. Wang and K. Komvopoulos: The multilayered structure of ultrathin amorphous carbon films synthesized by filtered cathodic vacuum arc deposition. *J. Mater. Res.* **28**, 2124 (2013).

Table I. Total thickness determined from TEM and EELS analyses, rms roughness, coefficient of friction, average sp^3 fraction in bulk layer, and residual stress of ~60-nm-thick single- and multi-layer *a*-C films.

Film type	Film thickness (nm)		Roughness (nm)	Coefficient of friction	sp^3 in bulk layer (%)	Residual stress (GPa)
	Measurement method					
	TEM	EELS				
single-layer	63.1	59.1	0.23 ± 0.02	0.17 ± 0.01	43.05 ± 0.90	7.20 ± 0.01
multi-layer	65.0	60.9	0.14 ± 0.01	0.13 ± 0.01	44.39 ± 1.59	3.26 ± 0.01

List of Figures

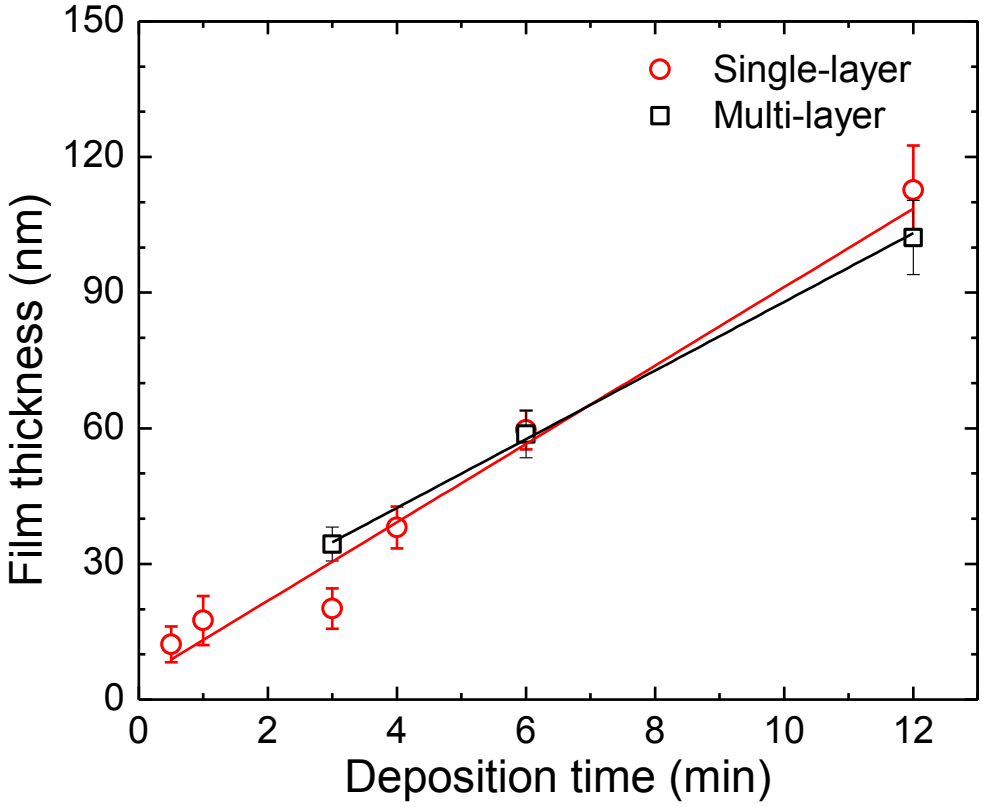
Single-layer
Multi-layer
Film thickness (nm)
Deposition time (min)
0
30
60
90
120
150
0
2
4
6
8
10
12

Figure 1

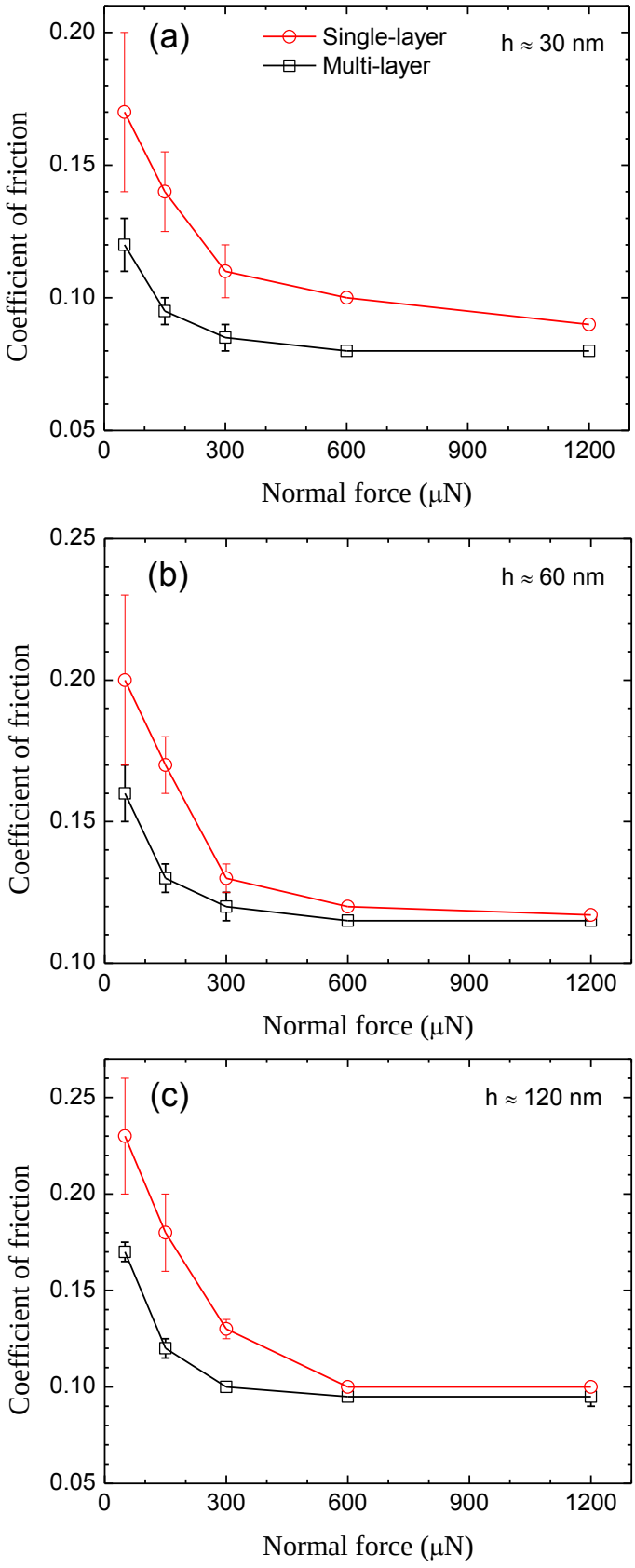
(a)
Single-layer
Multi-layer
h ≈ 30 nm
Coefficient of friction
0.20
0.15
0.10
0.05
0
300
600
900
1200
Normal force (μN)
(b)
h ≈ 60 nm
Coefficient of friction
0.25
0.20
0.15
0.10
0
300
600
900
1200
Normal force (μN)
(c)
h ≈ 120 nm
Coefficient of friction
0.25
0.20
0.15
0.10
0.05
0
300
600
900
1200
Normal force (μN)

Figure 2

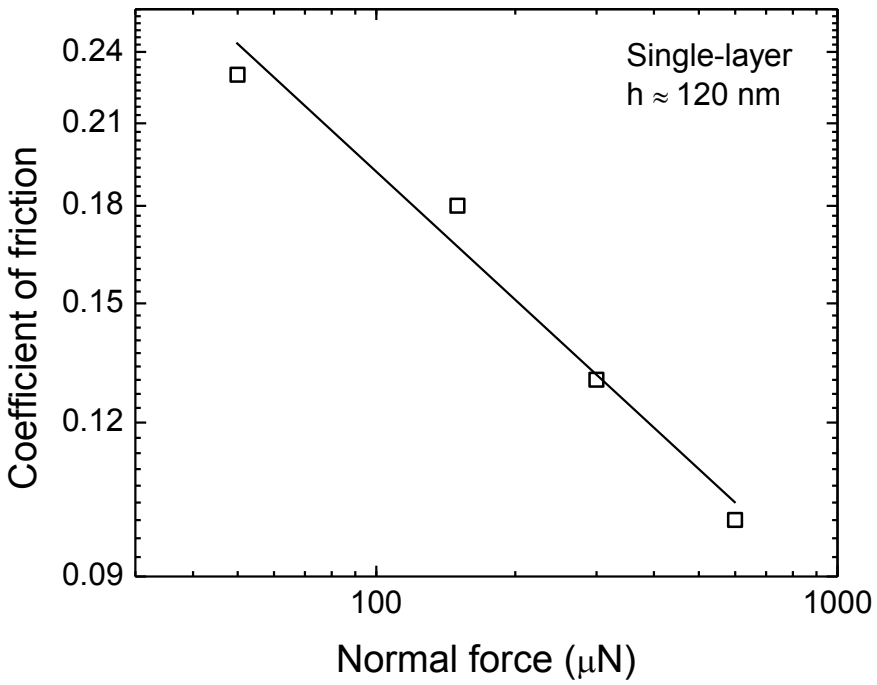
Single-layer
h ≈ 120 nm
Coefficient of friction
0.24
0.21
0.18
0.15
0.12
0.09
100
1000
Normal force (μN)

Figure 3

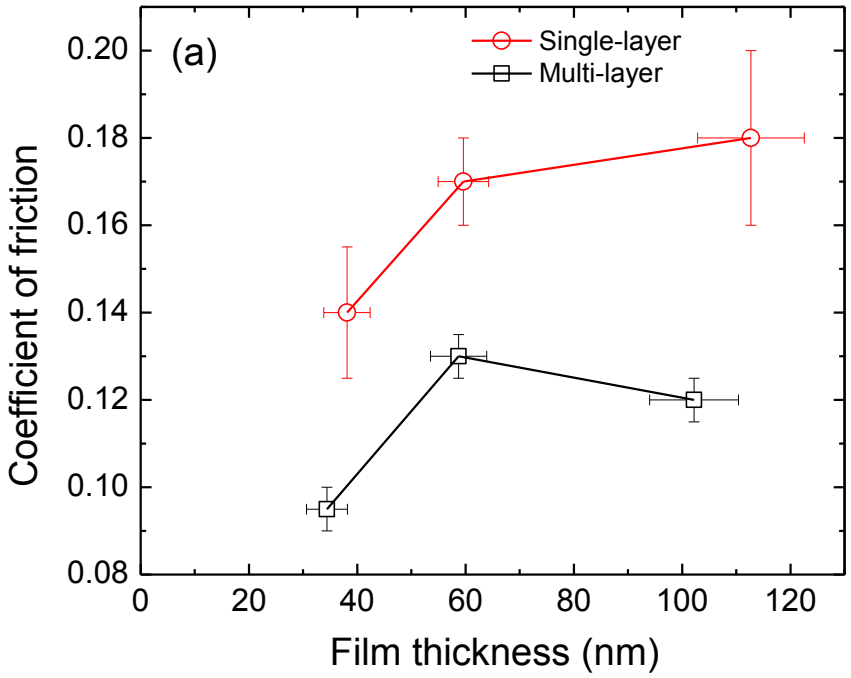
(a)
Single-layer
Multi-layer
Coefficient of friction
0.20
0.18
0.16
0.14
0.12
0.10
0.08
0
20
40
60
80
100
120
Film thickness (nm)

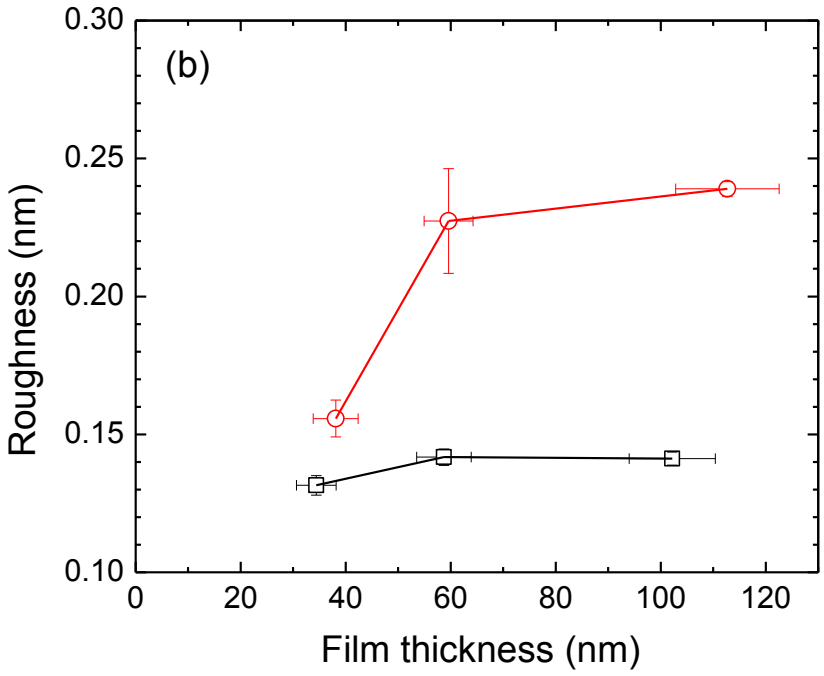
(b)
Roughness (nm)
0.30
0.25
0.20
0.15
0.10
0
20
40
60
80
100
120
Film thickness (nm)

Figure 4

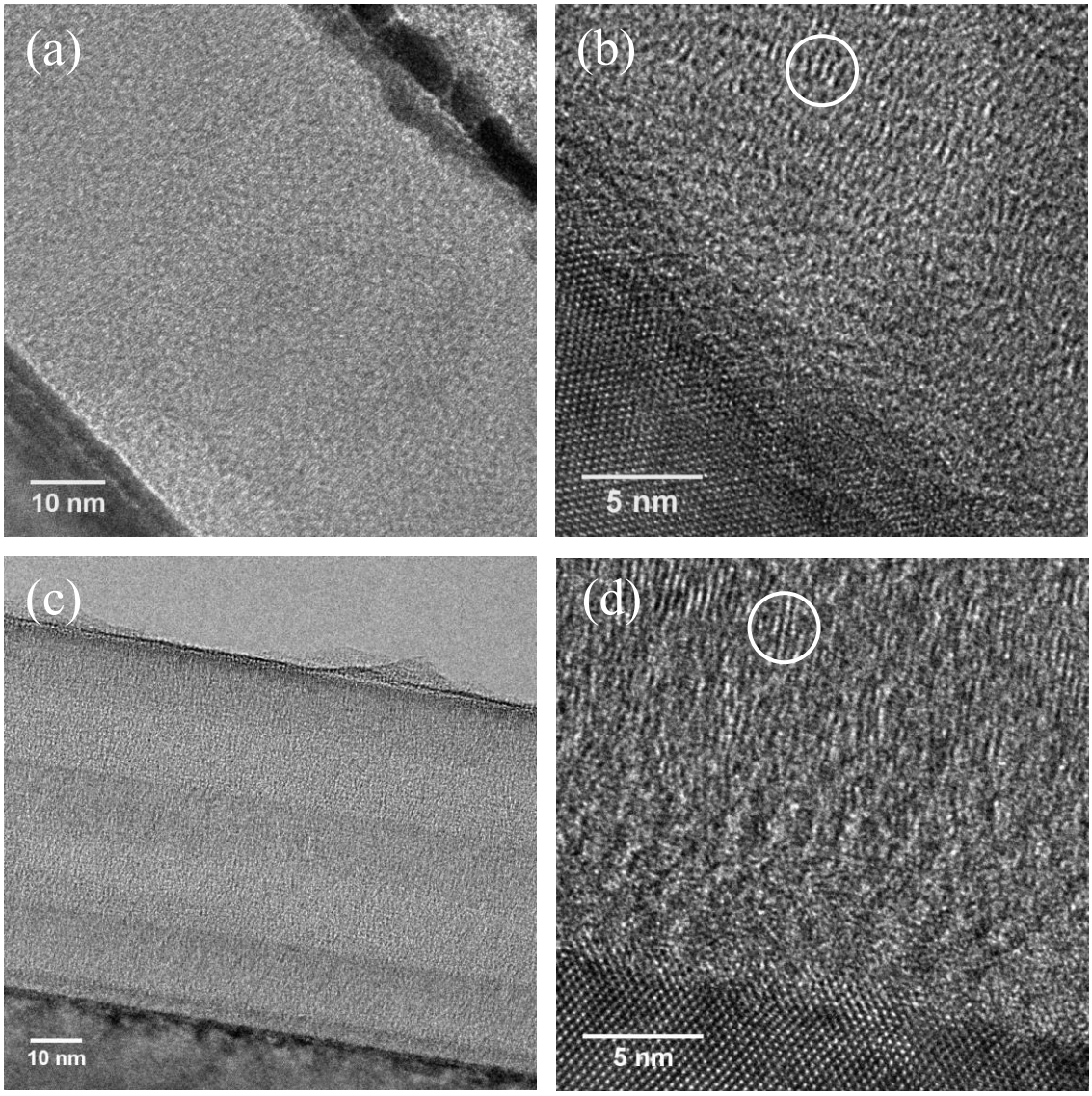

Figure 5

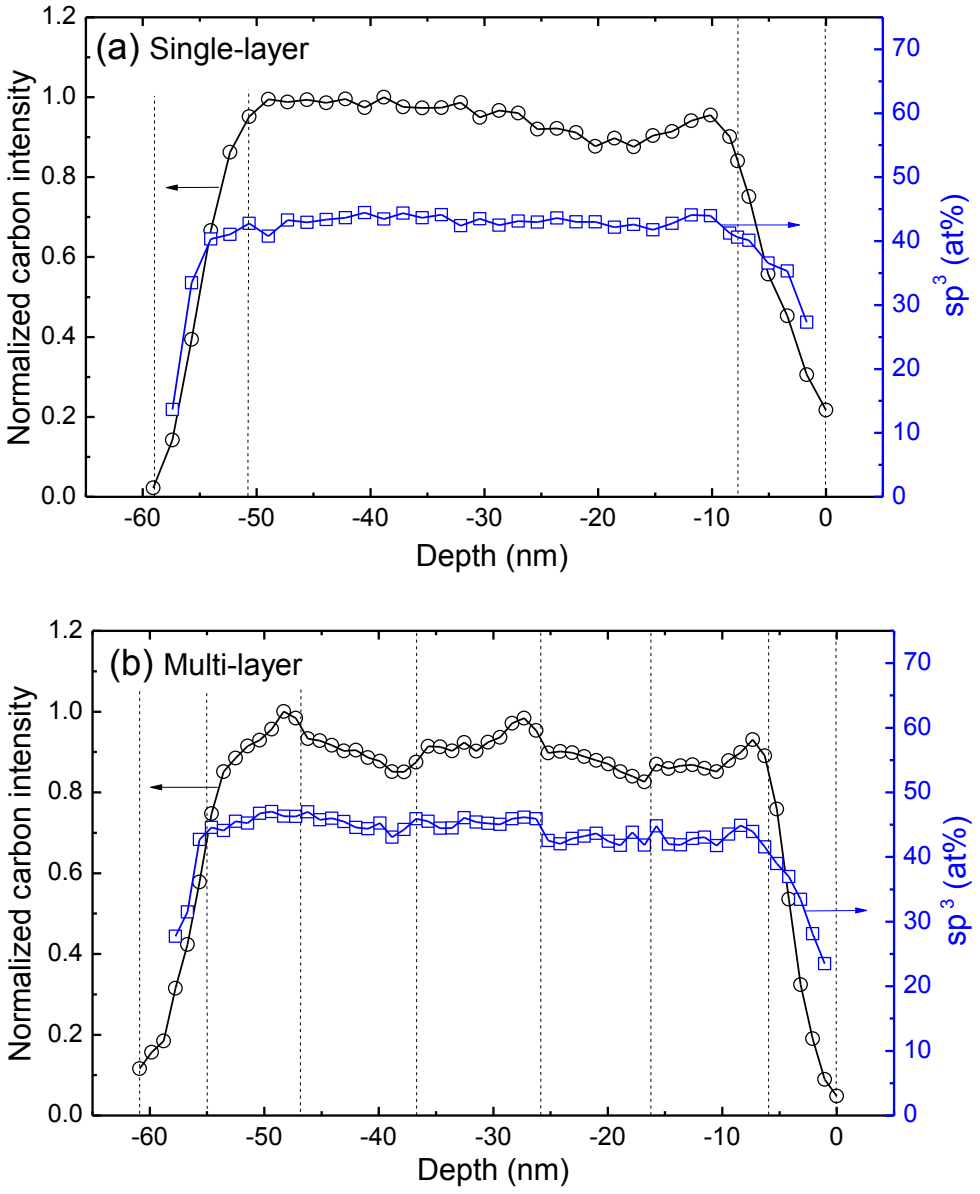
(a) Single-layer
Normalized carbon intensity
sp3 (at%)
Depth (nm)
(b) Multi-layer
Normalized carbon intensity
sp3 (at%)
Depth (nm)

Figure 6